

**Keywords:**

LiFe₅O₈,
Spinel,
Glycine-Nitrate Method,
Superparamagnetism,
Microstructure,
Anode

Received: June 5, 2017

Accepted: June 27, 2017

Published: August 29, 2017

Microstructure and Properties of Lithium Ferrite in the Process of Its Formation

Konstantin Zheleznikov, Elizaveta Shalaeva, Dina Kellerman*

Institute of Solid State Chemistry, Ural Branch, Russian Academy of Sciences, Ekaterinburg, Russia

Email address

kellerman@ihim.uran.ru (D. Kellerman)

*Corresponding author

Citation

Konstantin Zheleznikov, Elizaveta Shalaeva, Dina Kellerman. Microstructure and Properties of Lithium Ferrite in the Process of Its Formation. *American Journal of Materials Research*. Vol. 4, No. 3, 2017, pp. 15-22.

Abstract

LiFe₅O₈ has been synthesized by the self-propagating glycine-nitrate method. To clarify the stages of lithium ferrite phase formation, the structural, magnetic, and thermogravimetric studies have been carried out. The evolution of the magnetic properties indicated a transition from homogeneous distribution of iron ions in the carbon matrix to their clustering and subsequent crystallization of the magnetic lithium ferrite phase. The coexistence of α - and β - LiFe₅O₈ was found. The electrochemical tests showed a reduction of Fe³⁺ ions to metallic state during the lithiation process.

1. Introduction

The inversed spinel LiFe₅O₈ is known to crystallize in two polymorphic modifications: ordered (α , space group P_4332) and disordered (β , space group $Fd3m$). In the structure of the ordered low temperature phase all Li⁺ ions and three-fifth of all Fe³⁺ ions occupy the octahedral B-sites, while the remaining Fe³⁺ ions occupy the tetrahedral A-sites, so the formula can be written as (Fe³⁺)_{8c}[(Li_{0.5})_{4b}(Fe³⁺_{1.5})_{12d}]O₄. The disordered phase exists at higher temperatures ($T > 1020$ K) and is characterized by randomly distributed metal ions ((Fe³⁺)_{8a}[Li_{0.5}Fe³⁺_{1.5}]_{16d}O₄) [1]. As the temperature decreases, the reverse $\beta \rightarrow \alpha$ -transition occurs. To keep lithium ferrite in the disordered β -state, quenching from high temperatures is used [2].

Lithium ferrite, due to its high resistivity, high Curie temperature (620°C), a square hysteresis loop and high magnetization, has been extensively studied as a material for electrical components, memory cores, microwave devices, etc. A low cost, easy synthesis, temperature stability and a low toxicity make it an attractive substitute for garnets and other expensive functional materials [3]. LiFe₅O₈ is also interesting as an electrode material for lithium-ion batteries [4]. Moreover, lithium ferrite is considered both as an anode [5] and a cathode material [6]. According to [6, 7], the spinel LiFe₅O₈ shows promise as a cathode material for lithium ion batteries with a high rate capability and good cycling stability because lithium could be reversibly intercalated/deintercalated in and out of LiFe₅O₈. The LiFe₅O₈ spinel has been synthesized from different starting materials using different methods such as co-precipitation, sol-gel method, hydrothermal method, etc. [8-11]. One of the obstacles to the practical application of LiFe₅O₈ as an electrode material is its low intrinsic electronic conductivity resulting in a low capacity during cycling. There are many traditional approaches to solve this problem, such as partial replacement of iron ion by other elements [12] making small-sized particles [13],

etc. Among other approaches, the production of “electrode material/carbon” composites offers significant advantages for improving the transport properties of lithium ferrite [14]. In this work, we consider the synthesis and properties of lithium ferrite containing a considerable amount of amorphous carbon together with nano-crystallized graphite.

2. Experimental Details

LiFe₅O₈ ferrite samples have been prepared by the glycine-nitrate method. The chemicals used: iron (III) nitrate nonahydrate Fe(NO₃)₃ · 9H₂O, lithium carbonate Li₂CO₃, nitric acid HNO₃, amino acetic acid NH₂CH₂COOH (glycine) were of reagent grade quality. Weighed amounts of iron nitrate and lithium nitrate dissolved separately in distilled water were mixed together in the stoichiometric ratio Li:Fe = 1:5. Fuel (glycine) was added in the molar ratio 6:1 to the metal nitrates. Then the temperature of the resulting mixture was raised to 330°C until a combustion reaction occurred. The obtained intermediate product was ground and annealed at different temperatures in the range from 100 to 900°C in a muffle furnace for 1 h.

X-ray diffraction experiments for the samples before and after annealing were carried out at room temperature using a MAXima_X XRD-7000 SHIMADZU diffractometer (CuK_α radiation, 2θ range of 5-70 degrees, step of 0.03 deg). The phase composition of the samples was determined by comparing their XRD patterns with those in the PDF2 database (ICDD, USA, release 2009).

The scanning electron microscopy (SEM, JEOL JSM-6390 LA) and transmission electron microscopy (TEM, JEOL JEM-200CX) studies were performed to observe the particle morphology. The distribution of carbon, oxygen and iron was determined by energy dispersion X-ray (EDX) analysis with a JED 2300 analyzer. A transmission electron microscopy study was carried out in diffraction and imaging modes on a JEM-200CX device operating at a voltage of 160 keV. The microdiffraction patterns were obtained from regions ~200-500 nm in size. The samples suitable for electron diffraction analysis were prepared by 5 min ultrasonic dispersion in ethanol of the powders pre-crushed in a mortar. A few droplets of the ethanol suspension were deposited on a holey carbon Cu grid.

The magnetization curves were collected by means of a VSM-5T (Cryogenic Ltd.) vibrating sample magnetometer in the temperature interval from 2 to 300 K with magnetic field ranging between 0 and 50000 Oe.

The thermal analysis measurements were carried out with a SETARAM SETSYS Evolution 1750 apparatus in static air at a heating rate of 1°C/min.

The specific surface area of the samples was obtained using a Gemini VII Analyzer (Micromeritics) from the N₂ adsorption-desorption isotherms and was calculated by the Brunauer-Emmett-Teller (BET) method.

The electrochemical study on electrode was carried out on an MSTAT 4 (Arbin, USA) multi-channel electrochemical

test system in galvanostatic mode. An airtight flat two-electrode cell equipped with a counter consisting of lithium anode (99%, Sigma-Aldrich) supported on a copper substrate and a Celgard 2500 polypropylene separator was used. The positive electrodes for the cell were fabricated by pasting the slurry of the as-prepared lithium iron oxide powder (83%), acetylene black (10%) and polyvinylidene difluoride PVDF-Solef 5130 (7%) dissolved in N-methylpyrrolidone (NMP) on Al foil strips by the doctor blade technique. Then the strips were sliced in 32 mm diameter sections and dried at 90°C for 6 h in a vacuum oven to remove water impurity. The cells were assembled in an argon filled glove box (MBraunLabStar)*.

3. Results and Discussion

3.1. TG and XRD Characterization

When lithium pentaferriite is synthesized by the glycine-nitrate method, the product of the combustion reaction contains a large amount of organic residues including unreacted aminoacetic acid. The thermal gravimetric analysis was performed to determine the temperature of complete decomposition of the residues, as well as the temperature of LiFe₅O₈ phase formation. The results are presented in Figure 1. The thermal profile shows three distinct regions of weight loss. The first weight loss between 100 and 130°C can be attributed to vaporization of water from the agglomerates formed during the combustion reaction; the further weight loss at temperatures to 230°C is due to complete decomposition of glycine residues [15]; and the final loss occurs at 280 to 350°C and reflects complete removal of organic residues and atomic carbon. The material appears to be stable at T > 500°C. These conclusions are in good agreement with the X-ray diffraction results. The XRD patterns of the as-prepared (LFO-0) and heat-treated samples (hereafter designated as LFO-105, LFO-190, LFO-270, LFO-300, LFO-350 and LFO-900) are demonstrated in Figure 2. The corresponding weight losses of the heat-treated samples are marked in Figure 1 by asterisks. It is seen that the sample annealed at ~100°C, as well as the as-prepared sample contain a crystal phase of α-glycine. When the temperature is raised to 190°C, glycine completely decomposes to form an amorphous carbon matrix. The samples remain in X-ray amorphous state at T > 270°C. At 300°C, the LiFe₅O₈ phase begins to crystallize. This process takes place simultaneously with oxidation of carbon and its removal mostly in the form of CO₂.

* The authors are grateful to Dr. V. S. Gorshkov for carrying out the electrochemical measurements and for the helpful tips

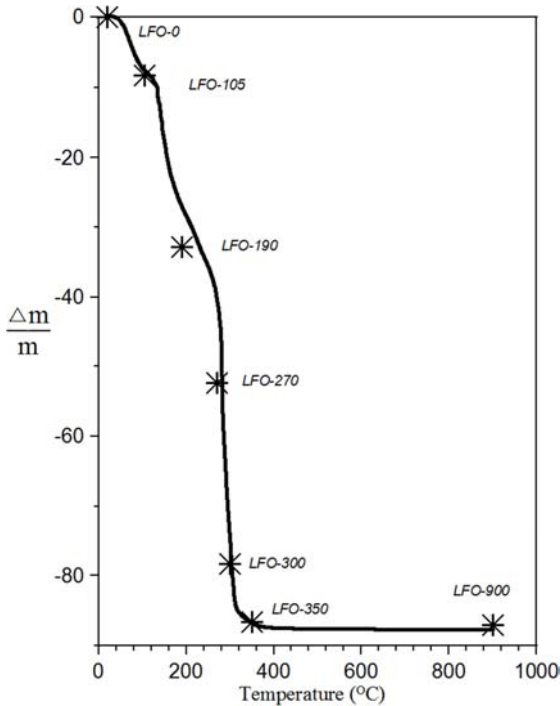


Figure 1. The TG curve of the as-prepared ferrite powder (LiFe_5O_8). Weight losses after heat treatment of the as-prepared sample at 105 C°, 190 C°, 270 C°, 300 C°, 350 C° and 900 C° are marked by asterisks.

3.2. Morphological Characterization

The specific surface area (S_{BET}) of the particles in the as-prepared sample is not very large (Table 1). The decomposition of organic residues accompanied by carbon removal leads to an increase in the specific surface area by more than two orders of magnitude during heating to 350°C. At high temperatures, the surface area of the ferrite particles decreases again as a result of sintering effect. Narrowing of the diffraction peaks at 900°C also indicates an increase in the crystallite size (Figure 2).

The SEM examination of the surface morphology shows that the growth of lithium pentaferrite particles begins at $T > 270^\circ\text{C}$. At lower temperatures, the surface appears as an undifferentiated crust formed obviously by carbon and organic residues (Figure 3a). This agrees well with the TG and XRD data (Figure 1, Figure 2). In the SEM micrographs for LFO-300 and LFO-350 (Figure 3d, 3e) one can see the macro-agglomerates of irregular shape corresponding to the crystalline phase of LiFe_5O_8 . In this case, the size of individual particles cannot be determined accurately. At higher annealing temperatures, the particles acquire a more regular shape and at 900°C become generally near spherical with a diameter of ~ 300 nm.

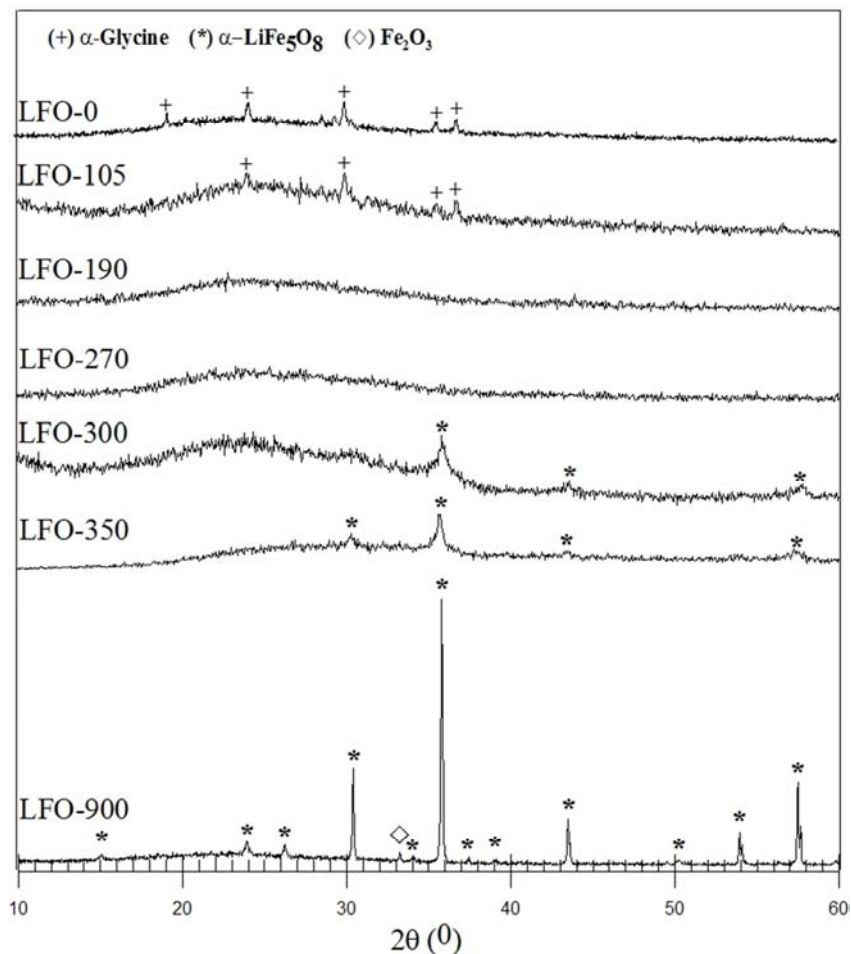


Figure 2. The X-ray diffraction patterns of as-prepared and heat-treated samples of LiFe_5O_8 : (1) as-prepared, (2) -105°C, (3)- 190°C, (4)- 270°C, (5)- 300°C, (6) -350°C, (7) -900°C. The corresponding diffraction peaks are labeled: + - α -glycine, * - LiFe_5O_8 .

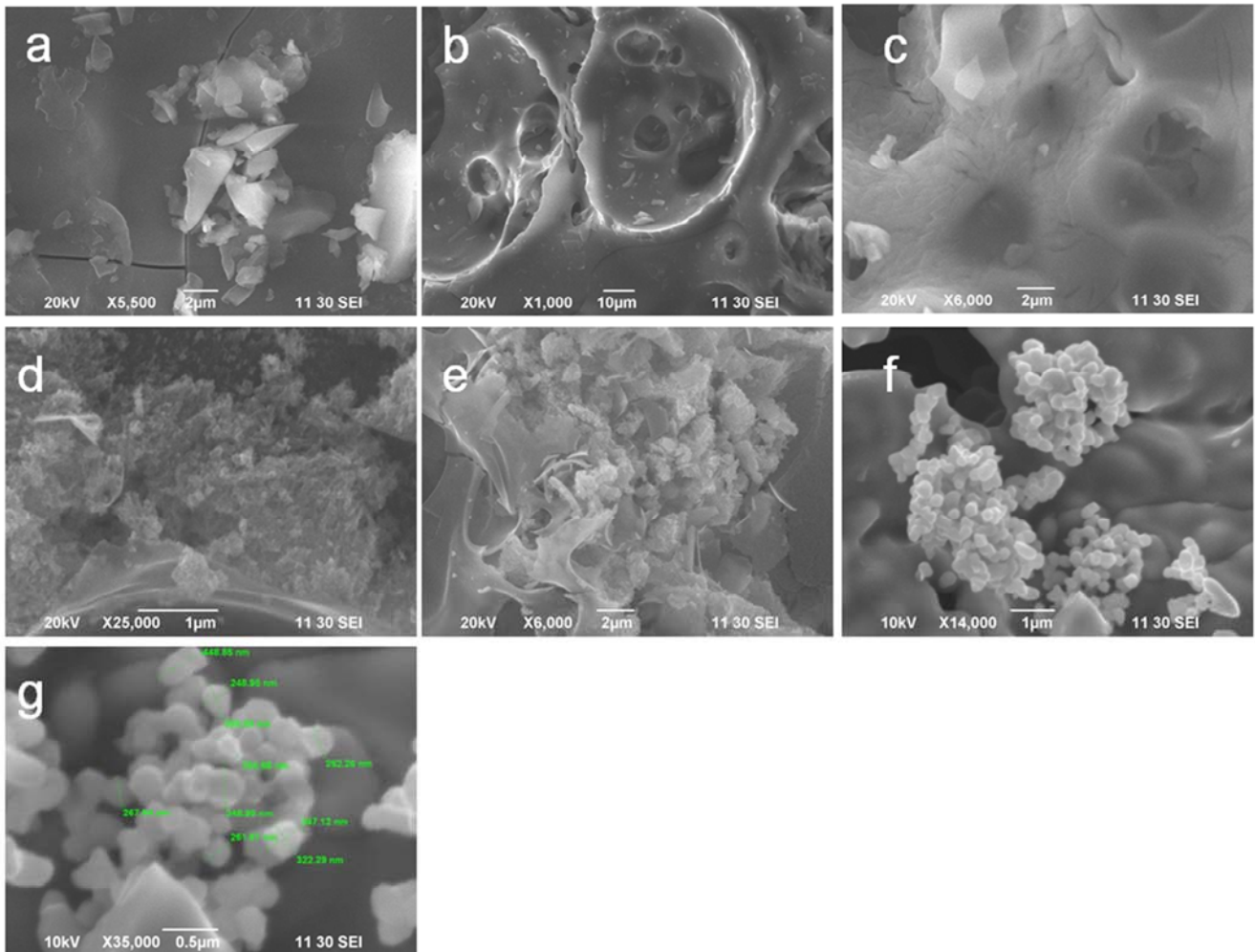


Figure 3. The SEM micrographs for heat-treated samples of “ LiFe_5O_8 ”: a -LFO-105, b -LFO-190, c -LFO-270, d -LFO-300, e-LFO-350, f-LFO-900; g-LFO-900 with marked particles.

Table 1. Variation in the specific surface area (S_{BET}) during LiFe_5O_8 phase formation.

Sample	$S_{\text{BET}}, \text{m}^2/\text{g}$
LFO-0	0.39 ± 0.02
LFO-105	0.31 ± 0.01
LFO-190	1.14 ± 0.02
LFO-270	3.15 ± 0.01
LFO-300	17.92 ± 0.07
LFO-350	35.24 ± 0.20
LFO-900	1.13 ± 0.06

3.3. TEM Characterization

To examine in more detail the microstructure of the samples comprising along with the final LiFe_5O_8 phase a certain amount of residual carbon, the TEM study of LFO-300 was performed.

The obtained data reveal that the LiFe_5O_8 particles with varying size are included into the carbon matrix of the test specimen. This is clearly seen from the bright-field electron microscopy image given in Figure 4a. Note that carbon is in amorphous as well as in crystalline state. There is a diffuse halo in the diffraction pattern (Figure 4b), which is typical of

amorphous carbon. The blurred Debye rings correspond to the strongest diffraction reflection of nanocrystalline graphite and to some reflections belonging to larger graphite particles (~100 nm). The electron diffraction pattern of nanocrystalline texturized graphite crystallized in an amorphous carbon film is presented for comparison (d). The diffraction pattern contains diffraction spots that can be identified as reflections from individual LiFe_5O_8 crystals (Figure 4b, 4c). It is evident from Figure 5 that the particles observed in area 1 of the bright-field microphotograph (Figure 5a) correspond to LiFe_5O_8 having a different structure (Figure 5b). In other words, the sample under consideration contains both modifications of LiFe_5O_8 : the ordered phase, which is thermodynamically stable at room temperature (s.g. P_4332), and the high-temperature disordered phase (s.g. $Fd-3m$). The non-equilibrium state of the system is confirmed by the presence of dislocation loops observed within some particles (Figure 6). The sample was also found to contain small crystallites of LiFeO_2 with a lattice parameter of 4.16Å (Figure 5a, indicated by arrows, Figure 5c - electron diffraction pattern).

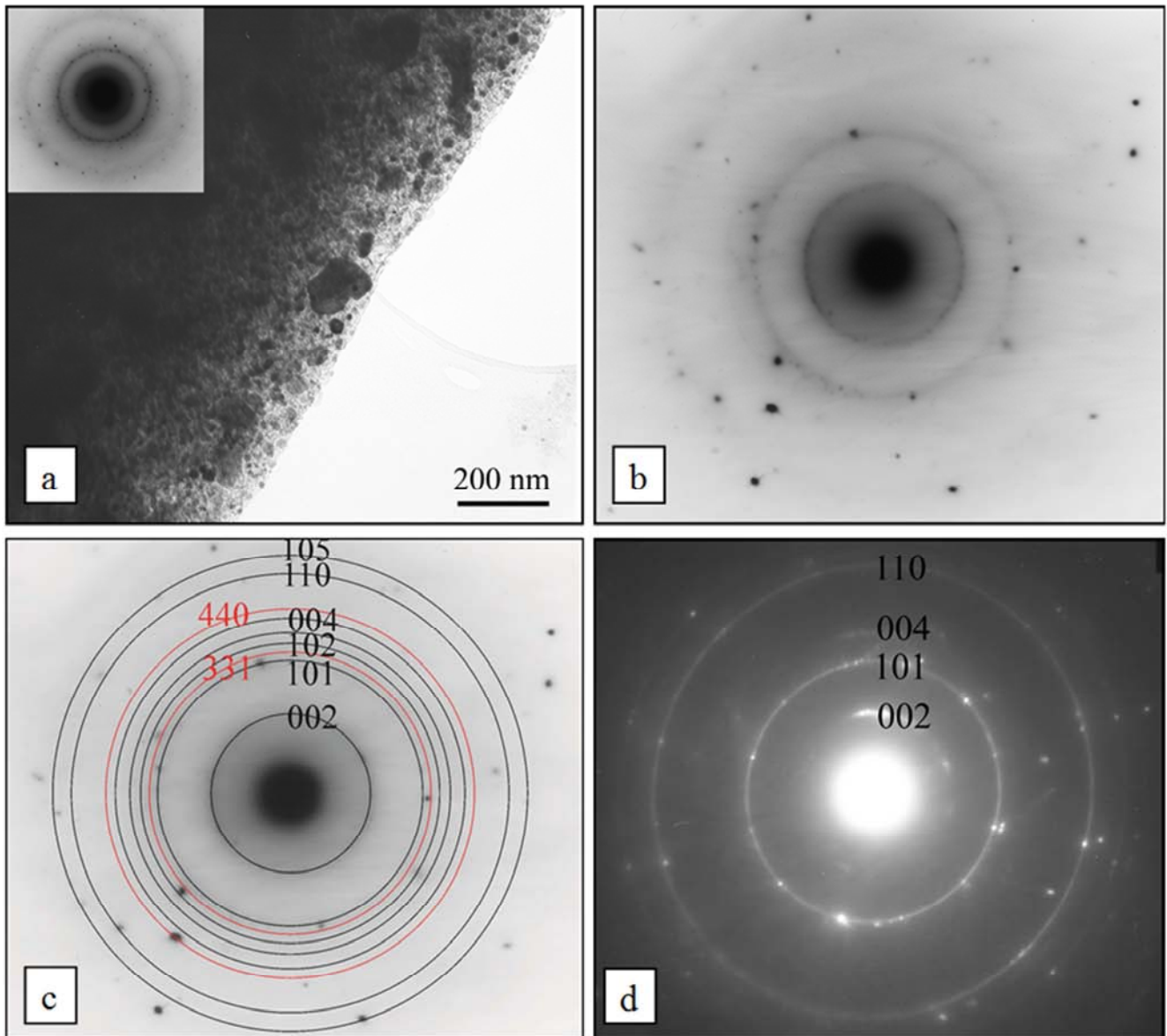


Figure 4. The bright-field TEM image (a), electron diffraction pattern (b) and its scheme (c) for LFO-350. Indexes of graphite (black) and spinel LiFe_5O_8 (Fd-3m) are indicated. The electron diffraction pattern of the nanocrystalline texturized graphite crystallized in amorphous carbon film (d).

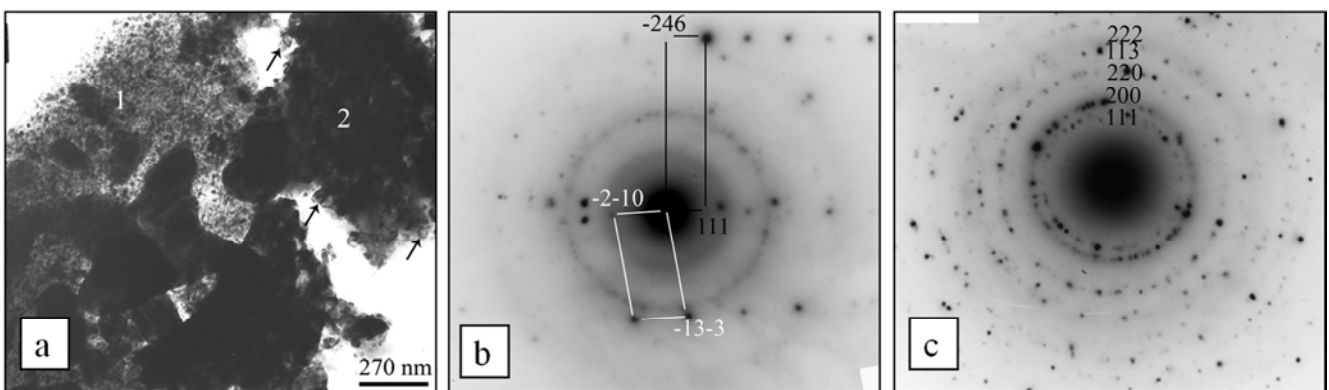


Figure 5. The bright-field TEM image obtained from multiphase area (a); the electron diffraction pattern from field 1 containing two modifications of LiFe_5O_8 : (Fd-3m, black lines); (P,332, white lines) (b); the electron diffraction pattern from field 2 containing LiFeO_2 (Fm3m)(c).

3.4. Magnetic Measurements

Since LiFe_5O_8 is a ferromagnet with a high Curie temperature, its formation clearly manifests itself in the magnetic properties. Variations of room temperature magnetization with applied magnetic field for the samples prepared by glycine-nitrate method and heat-treated at different temperatures are presented in Figure 7. The results of magnetic measurements show that up to the annealing temperature of 300°C , all samples are paramagnetic and their magnetization is a linear function of the applied field. The paramagnetic behavior indicates that at these temperatures the iron and lithium ions are uniformly distributed in the amorphous carbon matrix and no crystallization of magnetic spinel (LiFe_5O_8) occurs. As the annealing temperature increases above 300°C , the particles of the magnetic phase LiFe_5O_8 begin to form in a diamagnetic graphite matrix, as evidenced by the measured magnetization curves. This is in good agreement with the XRD data (Figure 2). The higher is the temperature of heat treatment, the more intensive is the process of magnetic phase formation and the higher is the value of saturation magnetization (Figure 7).

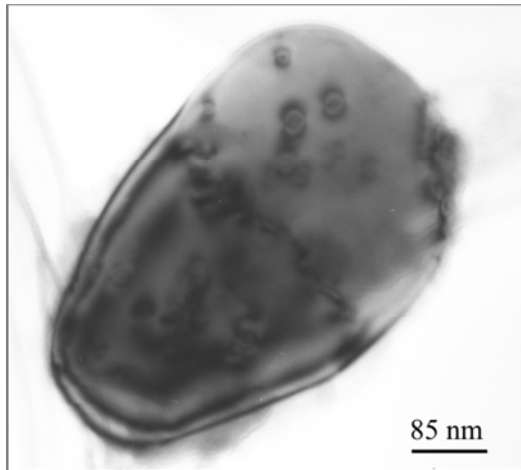


Figure 6. The dislocation loops in the particle of LiFe_5O_8 .

At the initial stages of pentaferrite formation, the appearing magnetic particles are isolated from each other by a diamagnetic interlayer and such system is characterized by a superparamagnetic behavior. This can be clearly seen from the temperature dependence of magnetization shown for LFO-300 in Figure 8. The following measurement procedure was used: the samples were cooled to 1.5 K in the absence of external magnetic field; then measurements at a magnetic field of 100 Oe were carried out upon heating (ZFC mode). The sample was re-cooled at a magnetic field of 100 Oe and then the measurements were performed upon heating in the same field (FC mode). The superparamagnetic behavior of the system manifests itself primarily in the divergence between the magnetization curves measured in the FC and ZFC conditions. While the FC magnetization increases continuously with the temperature and then remains almost constant, the ZFC magnetization decreases after the maximum value has been

reached. The maximum in the ZFC dependence correlates with the blocking temperature (T_{block}) related to magnetic anisotropy (k_{eff}) and particle volume (V) by the ratio $k_{\text{eff}} \cdot V = 25k_B \cdot T_{\text{block}}$. Below T_{block} , the anisotropy energy is larger than the thermal energy and blocks the alignment of the moments in the direction of the applied field. If we consider the LiFe_5O_8 particles as spherical and take the values of $k_{\text{eff}} = 9000 \text{ J / m}^3$ [16] and $T_{\text{block}} = 275 \text{ K}$ (Figure 5), we can calculate that the radius of the particles in LFO-300 is $\approx 35 \text{ nm}$. As follows from the microscopic data, these small particles are assembled mainly into agglomerates. In addition, there is a large variation in the particle size, which explains the fact that the LFO-300 sample demonstrates not only superparamagnetic behavior, but also a hysteresis loop.

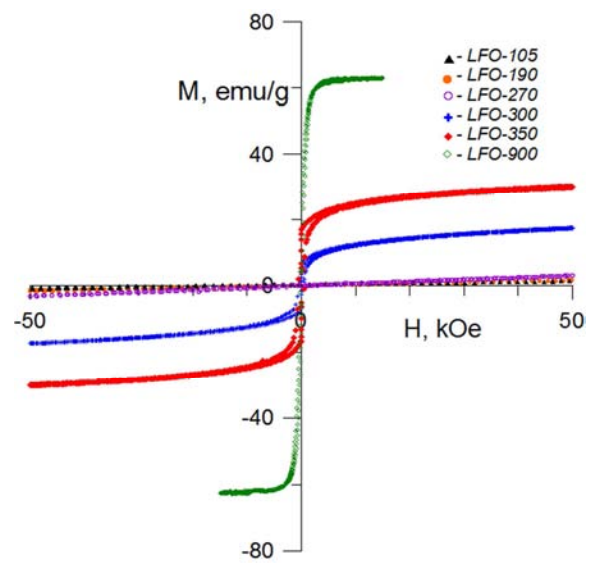


Figure 7. The magnetization versus applied magnetic field curves for the heat-treated samples of LiFe_5O_8 precursor obtained by glycine-nitrate method.

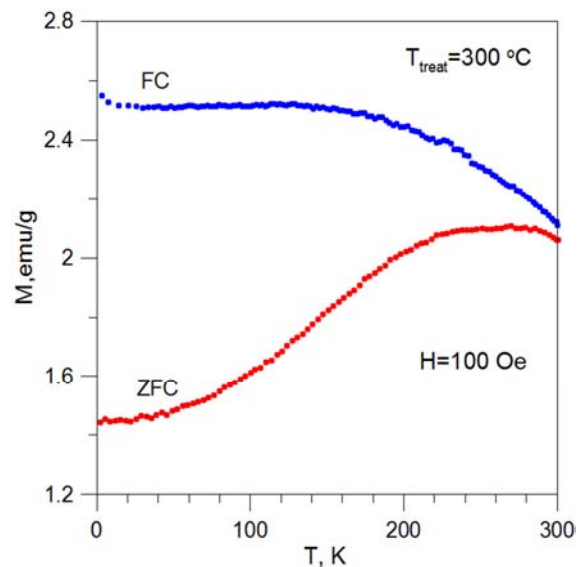


Figure 8. The zero-field cooled (ZFC) and field cooled (FC) curves for LFO-300 recorded in a magnetic field of 100 Oe.

3.5. Electrochemical Tests

The galvanostatic charge–discharge curves of LiFe_5O_8 composite electrode (LFO-300) were obtained at a current density of 13 mA g^{-1} in the potential range 0.6 - 4 V. The first discharge curve rapidly decreases to 0.8 V (Figure 9) and exhibits a lingering voltage plateau (Figure 9). The obtained capacity value ($\approx 1700 \text{ mA}\cdot\text{h/g}$) allows us to suppose that the discharge products contain more lithium than can be predicted by simple charge counting and that the electrochemical reaction of lithiation differs from the classical Li insertion/deinsertion mechanism.

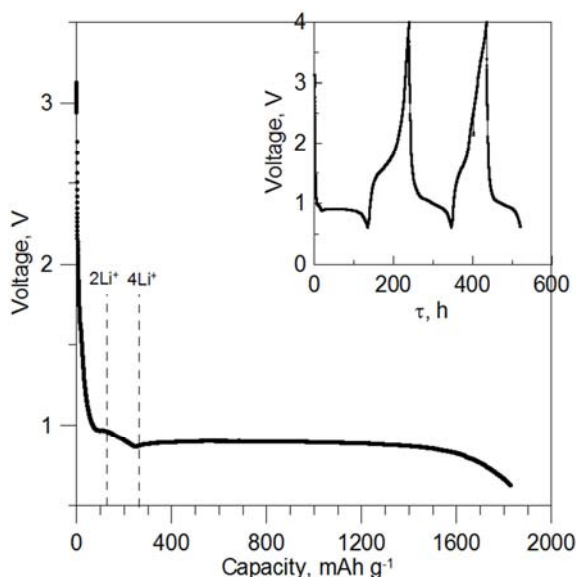


Figure 9. Voltage vs. capacity of LFO-300 sample for the first voltage range 0.6–4 V. Inset: the charge–discharge curves of Li/LFO-300.

The bends observed in the curve indicate that in the first cycle the lithium insertion proceeds through different stages and the first discharge curves can be described by successive electrochemical reactions. Judging by the inflection point, the first stage consists in joining of two lithium ions: $\text{LiFe}^{3+}_5\text{O}_8 + 2\text{Li}^+ = \text{Li}_3\text{Fe}^{2.6+}_5\text{O}_8 - 2e^-$. This reversible reaction depicts a typical behavior of LiFe_5O_8 with the oxidation state of iron switching between +3 and +2.6 due to lithium intercalation [7]. The theoretical capacity of this process is $130 \text{ mA}\cdot\text{hrs/g}$. According to Ref. [17], these lithium ions occupy the 16c spinel position. The next bend is fixed at the capacity of about $260 \text{ mA}\cdot\text{h/g}$ and therefore the introduction of two more Li^+ can be assumed: $\text{Li}_3\text{Fe}^{2.6+}_5\text{O}_8 + 2\text{Li}^+ \rightarrow \text{Li}_5\text{Fe}^{+2.2}_5\text{O}_8 - 2e^-$. In this case additional Li atoms can enter into the 48f spinel sites [18] and the phase with equiatomic content of lithium and iron, which is likely to be structurally related to the tetragonal lithium ferrite LiFeO_2 , eventually forms [19]. Further Li insertion corresponds to the plateau on the voltage profile. At this stage, lithium reacts with the oxide to form lithium oxide and iron metal. The reaction can occur in accordance with the equation $\text{Li}_5\text{Fe}_5\text{O}_8 + 11 \text{Li}^+ \rightarrow 8\text{Li}_2\text{O} + 5\text{Fe}^0 - 11 e^-$. Reversible reduction of the iron ions to the metallic state makes it possible to achieve a high electrode capacity of lithium ion battery with iron oxide electrode and therefore is of great interest [20–24].

The theoretical capacity that can be achieved as a result of complete electrochemical reduction of iron in LiFe_5O_8 should be $975 \text{ mA}\cdot\text{h/g}$. However, the capacity at the first discharge was measured to be much higher than the theoretical value (Figure 9). This value of the discharge capacity is practically the same as given in Ref. [24] for carbon coated nanocrystalline porous $\alpha\text{-LiFeO}_2$. The extra capacity as compared with that predicted by the equation $\text{LiFe}_5\text{O}_8 + 15 \text{Li}^+ \rightarrow 8\text{Li}_2\text{O} + 5\text{Fe}^0 - 15 e^-$ is due most likely to catalytic electrolyte decomposition reactions [25] or to further lithium storage via interfacial reaction caused by the charge separation at the metal/ Li_2O interface [26]. The reverse reaction related to the decomposition of Li_2O accompanied by oxidation of Fe nanoparticles takes place, but the discharge capacity of the second cycle is already 1.5 times smaller than for the initial cycle. In the subsequent cycles, the capacity tends to decrease further (Figure 9, inset). Nevertheless we believe that the cyclability can be improved by decreasing the lithium ferrite particle size and by optimization of the $\text{LiFe}_5\text{O}_8/\text{C}$ ratio.

4. Conclusions

Lithium ferrite LiFe_5O_8 was synthesized by the self-propagating glycine-nitrate method. To clarify the phase formation stages, the structural, magnetic, and thermogravimetric studies were carried out. It was shown that the LiFe_5O_8 phase begins to crystallize at $T \approx 280^\circ\text{C}$ and at low temperatures the α - and β -forms of LiFe_5O_8 coexist. Before the formation of LiFe_5O_8 begins, the system is paramagnetic. At the initial stages of LiFe_5O_8 crystallization, when isolated nano-sized magnetic particles appear in the carbon matrix, a superparamagnetic behavior is observed. The electrochemical tests showed a partially reversible reduction of the Fe^{3+} ions to the metallic state during the lithiation process.

Acknowledgements

This work was financially supported by the Ural Branch of the Russian Academy of Sciences (Grant No. 15-6-3-18).

References

- [1] P. B. Braun, A Superstructure in Spinel, *Nature* 170 (1952) 1123.
- [2] W. Cook, M. Manley, Raman characterization of α - and β - LiFe_5O_8 prepared through a solid-state reaction pathway, *J. of Solid State Chemistry* 183 (2010) 322–326.
- [3] P. D. Baba and G. M. Argentina, “Microwave lithium ferrites: An overview,” *IEEE Transactions Microwave Theory and Techniques*, Vol. 22, pp. 652–658, June 1974.
- [4] F. O. Ernst, H. K. Kammler, A. Roessler, S. E. Pratsinis <http://www.sciencedirect.com/science/article/pii/S0254058406002136> - cor1 mailto:pratsinis@ptl.mavt.ethz.ch, W. J. Stark, J. Ufheil, P. Novák, Electrochemically active flame-made nanosized spinels: LiMn_2O_4 , $\text{Li}_4\text{Ti}_5\text{O}_{12}$ and LiFe_5O_8 , *Materials Chemistry and Physics* 101 (2007) 372–378.

- [5] P. Prosini, M. Carewska, S. Loreti, C. Minarini, S. Passerini, Lithium iron oxide as alternative anode for Li-ion batteries, *Int. J. of Inorganic Materials* 2 (2000) 365–370.
- [6] W. Zhou, Y. Wang, L. Zhang, G. Song and S. Cheng, Capacitive nanosized spinel α -LiFe₅O₈ as high performance cathodes for lithium-ion batteries, *Int. J. Electrochem. Sci.*, 10 (2015) 5061-5068.
- [7] M. Catti, M. Montero-Campillo, First-principles modelling of lithium iron oxides as battery cathode materials, *J. Power Sources* 196 (2011) 3955-3961.
- [8] M. Vucinic-Vasic, B. Antic, J. Blanusa, S. Rakic, A. Kremenovic, A. S. Nikolic, A. Kapor, Formation of nanosize Li-ferrites from acetylacetonato complexes and their crystal structure, microstructure and order–disorder phase transition, *Appl. Phys. A* 82 (2006) 49–54.
- [9] B. Li, Y. Xieb, et al., Synthesis of the nanocrystalline α -LiFe₅O₈ in a solvothermal process, *Solid State Ionics* 120 (1999) 251–254.
- [10] M. Tabuchi, A. Nakashima, et al. Fine Li_{(4-x)/3}Ti_{(2-2x)/3}Fe_xO₂ (0.18 ≤ x ≤ 0.67) powder with cubic rock-salt structure as a positive electrode material for rechargeable lithium batteries, *J. Mater. Chem.*, 13 (2003) 1747-1757.
- [11] S. Verma, P. Joy, Low temperature synthesis of nanocrystalline lithium ferrite by a modified citrate gel precursor method, *Mater. Res. Bull.*, 43 (2008) 3447-3456.
- [12] K. Ding, J. Zhao, M. Zhao, Y. Chen, Y. Zhao, J. Zhou, The Effect of Ti Doping on the Electrochemical Performance of Lithium Ferrite, *Int. J. Electrochem. Sci.*, 11 (2016) 2513-2524.
- [13] W. Zhou, Y. Wang, L. Zhang, G. Song and S. Cheng Capacitive Nanosized Spinel α -LiFe₅O₈ as High Performance Cathodes for Lithium-ion Batteries, *Int. J. Electrochem. Sci.*, 10 (2015) 5061-5068.
- [14] R. Singhal, A. Kumar, R. S. Katiyar, Nanomaterials for Li Ion Rechargeable Batteries: Synthesis and Characterizations, *Journal of Nano Energy and Power Research*, 2 (2013). 25-40.
- [15] A. Mukasyan, P. Epstein, P. Dinka, Solution combustion synthesis of nanomaterials, *Proceedings of the Combustion Institute* 31 (2007) 1789–1795.
- [16] H. Yang, Z. Wang, L. Song, M. Zhao, J. Wang, H. Luo, A study on the coercivity and the magnetic anisotropy of the lithium ferrite nanocrystallite, *Phys. D: Appl. Phys.* 29, (1996) 2574-2578.
- [17] M. Pernet, P. Strobel, Lithium insertion into iron spinel, *Defect and Diffusion Forum Vols 127-128* (1995) 73-92.
- [18] C. Chen, M. Geenblattj, J. V. Waszczak, Lithium Insertion Compounds of LiFe₅O₈, Li₂FeMn₃O₈, and Li₂ZnMn₃O₈, *J. of Solid State Chemistry* 64 (1986) 240-248.
- [19] Y. Lee, C. Yoon, Y. S. Lee, Y.-K. Sun, Synthesis and structural changes of Li_xFe_yO_z material prepared by a solid-state method, *J. of Power Sources* 134 (2004) 88–94.
- [20] I. Uzunov S. Uzunova, D. Kovacheva, S. Vasilev, B. Puresheva, Iron-based composite oxides as alternative negative electrodes for lithium-ion batteries, *J. Mater. Sci.* 42 (2007) 3353–3357.
- [21] M. Obrovac, R. Dunlap, R. J. Sanderson, and J. R. Dahn, The electrochemical displacement reaction of lithium with metal oxides, *J. of The Electrochemical Society*, 148 (2001) A576-A588.
- [22] M. Thackeray, M. Chan, L. Trahey, S. Kirklin, and C. Wolverton., Vision for designing high-energy, hybrid Li ion/Li–O₂ cells, *J. Phys. Chem. Lett.* 4 (2013) 3607–3611.
- [23] L. Trahey, C. Johnson, et al., Activated lithium-metal-oxides as catalytic electrodes for Li–O₂ Cells, *Electrochemical and Solid-State Letters*, 14 (5) (2011) A64-A66.
- [24] M. Rahman., J. Wang, M. F. Hassan, Z. Chen, H.-K. Liu, Synthesis of carbon coated nanocrystalline porous α -LiFeO₂ composite and its application as anode for the lithium ion battery, *J. of Alloys and Compounds* 509 (2011) 5408–5413.
- [25] A. Ponroucha, P.-L. Taberna, P. Simon, M. R. Palacin. On the origin of the extra capacity at low potential in materials for Li batteries reacting through conversion reaction, *Electrochimica Acta* 61 (2012) 13–18.
- [26] J. Jamnik, J. Maier, Nanocrystallinity effects in lithium battery materials. Aspects of nanoionics. Part IV, *Phys. Chem. Chem. Phys.* 5 (2003) 5215–5220.